Formation of Densely Packed Single-Walled Carbon Nanotube Assembly

Cheol-Min Yang, Dong Young Kim, and Young Hee Lee*

BK21 Physics Division, Institute of Basic Science, Center for Nanotubes and Nanostructured Composites, Sungkyunkwan University, Suwon 440-746, Republic of Korea

Received April 4, 2005. Revised Manuscript Received July 26, 2005

Densely packed assemblies of single-walled carbon nanotubes (SWCNTs) were characterized by N_2 and CO_2 adsorption techniques. We presented a convenient method for forming densely packed assembly structures of SWCNTs. The SWCNTs were treated with mixtures of HNO_3/H_2SO_4 or H_2O_2/H_2SO_4 before and after purification, to control the packing density and porosity of the SWCNT samples. H_2O_2/H_2SO_4 treatment caused a dramatic increase in microporosity without significantly changing the mesoporosity, whereas HNO_3/H_2SO_4 treatment decreased the mesoporosity and simultaneously increased the microporosity. This reduced mesoporosity originates from the contraction of the interbundle distance of SWCNTs. After HNO_3/H_2SO_4 treatment of the purified SWCNTs, the micropore surface area increased about 8.6 times compared to the pristine sample, and the volume fraction of the micropores increased from 10% to 91%, indicating formation of densely packed assemblies of SWCNTs. Therefore, HNO_3/H_2SO_4 treatment could control not only the SWCNT bundle size but also the interbundle distance of the SWCNTs. Moreover, the purification is of importance in promoting the formation of densely packed SWCNTs. We also demonstrated that acid treatments could develop narrow micropores, which was evidenced by CO_2 adsorption at 273 K. We emphasize that this approach can simply control the packing density as well as the porosity of SWCNT assemblies.

Introduction

Carbon nanotubes[1] have great potential for their applications in nanotechnological fields. In particular, the reversible storage of supercritical gases such as H_2 and CH_4 on carbon-nanotube-related materials has attracted much attention in the areas of energy and environmental protection.[2−4] The efficient storage of supercritical gases using nanoporous materials has been widely studied as a realistic alternative to the compression storage technique. Single-walled carbon nanotube (SWCNT) assemblies have been proposed as a promising material for gas adsorption and storage.[2,5] Such assemblies provide various pore structures such as microporosity, mesoporosity, and macroporosity, which are governed by the diameter, tip opening, and assembling of the nanotubes.[6,7] Gas molecules can be accommodated within the inner empty spaces of individual tubules and interstitial spaces of SWCNT bundles. The interstitial spaces of SWCNT assemblies are directly related to the bundle size and interbundle distance of the SWCNTs. Therefore, it is necessary to control both the interstitial and internal spaces to obtain an appropriate porous SWCNT assembly for each specific application.

For use as energy storage devices such as supercapacitors, SWCNTs must provide a high surface area and high microporosity. Previous reports, however, have not shown high surface area and micropore volume.[8,9] Moreover, SWCNT assemblies should provide a high packing density for application to supercritical gas storage,[10] and yet, very low packing densities have been found because of the large interbundle distances caused by weak interbundle interactions.[6,7] The packing density and pore size distribution of porous nanostructured materials are very important factors in applications to supercritical gas storage media. Therefore, an optimal porosity design of SWCNT assemblies for such an application is highly desired.

According to the results by Bekyarova et al., single-walled carbon nanohorns (SWCNHs), whose tips and side walls were opened through O_2 oxidation, were compressed by applying high pressure to obtain nanoporous carbon with a high packing density.[11] This densely packed SWCNHs showed a high CH_4 storage capacity of 160 $cm^3\ cm^{-3}$ at 3.5 MPa and 303 K, exceeding the U.S. Department of Energy (DOE) target of 150 $cm^3\ cm^{-3}$ for practical use as storage

* To whom correspondence should be addressed. Fax: +82-31-290-5954. E-mail: leeyoung@skku.edu.

(1) Iijima, S. *Nature (London)* **1991**, *354*, 56.
(2) Lee, S. M.; An, K. H.; Lee, Y. H.; Seifert, G.; Frauenheim, T. *J. Am. Chem. Soc.* **2001**, *123*, 5059.
(3) Bekyarova, E.; Murata, K.; Yudasaka, M.; Kasuya, D.; Iijima, S.; Tanaka, H.; Kanoh, H.; Kaneko, K. *J. Phys. Chem. B* **2003**, *107*, 4681.
(4) Yang, C.-M.; Noguchi, H.; Murata, K.; Yudasaka, M.; Hashimoto, A.; Iijima, S.; Kaneko, K. *Adv. Mater.* **2005**, *17*, 866.
(5) Liu, C.; Fan, Y. Y.; Liu, M.; Cong, H. T.; Cheng, H. M.; Dresselhaus, M. S. *Science* **1999**, *286*, 1127.
(6) Yang, C.-M.; Kaneko, K.; Yudasaka, M.; Iijima, S. *Nano Lett.* **2002**, *2*, 385.
(7) Cinke, M.; Jing, L.; Chen, B.; Cassell, A.; Delzeit, L.; Han, J.; Meyyappan, M. *Chem. Phys. Lett.* **2002**, *365*, 69.
(8) Eswaramoorthy, M.; Sen, R.; Rao, C. N. R. *Chem. Phys. Lett.* **1999**, *304*, 207.
(9) Zhang, X.; Wang, W.; Chen, J.; Shen, Z. *Langmuir* **2003**, *19*, 6088.
(10) Menon, V. C.; Komarneni, S. *J. Porous Mater.* **1998**, *5*, 43.
(11) Bekyarova, E.; Kaneko, K.; Yudasaka, M.; Murata, K.; Kasuya, D.; Iijima, S. *Adv. Mater.* **2002**, *14*, 973.

10.1021/cm0507157 CCC: $30.25
Published on Web 11/09/2005

media.[3] As for the pore size, Kaneko et al. reported adsorption of supercritical N_2 and CH_4 on five kinds of activated carbon fibers (ACFs) with different micropore widths ranging from 0.75 to 1.45 nm.[12] The fractional filling of N_2 and CH_4 on each ACF, which is the ratio of the volume occupied by adsorbed N_2 and CH_4 to the micropore volume, increased with decreasing average micropore width. Therefore, high packing density and narrow microporosity of nanoporous materials should greatly facilitate the storage capacity of the supercritical gases.

In this study, we report the formation of densely packed SWCNT assembly structures with high microporosity. Treatments of HiPco SWCNTs with a mixture of nitric acid (HNO_3)/sulfuric acid (H_2SO_4) were performed before and after purification in order to control the packing density and porosity of the SWCNT assembly. The effects of the treatments on changes of the packing density and porosity of the SWCNT assemblies were investigated by N_2 (77 K) and CO_2 (273 K) adsorption, because the physisorption of gases on SWCNTs has been demonstrated to be a key technique for confirming the packing density and the pore structure of an SWCNT assembly.

Experimental Section

Purification of HiPco SWCNTs. HiPco SWCNTs were purchased from Carbon Nanotechnologies, Inc. Before analysis, the SWCNTs were immersed in ethanol to consider the aggregation effect of nanotubes in solution (pristine SWCNTs). The SWCNTs were heated in an air flow of 50 mL min^{-1} at 623 K for 1 h. The heat-treated SWCNTs were immersed in 35% hydrochloric acid (HCl) and stirred at room temperature for 12 h twice. The precipitates were filtered and then washed with distilled water several times. After the sample had been dried in a vacuum for 12 h at 383 K, it was heated in Ar atmosphere at 1173 K for 1 h [purified SWCNTs (yield 40 wt %)].

Acid Treatments of the Pristine and Purified HiPco SWCNTs. Purified SWCNTs (50 mg) were immersed and stirred at room temperature in 100 mL of a mixture of H_2O_2 (30%) and H_2SO_4 (97%) or HNO_3 (60%) and H_2SO_4 (97%) with a volume ratio of 1:9 for 48 h [pu-H_2O_2/H_2SO_4-48 h (yield 92 wt %) and pu-HNO_3/H_2SO_4-48 h (yield 84 wt %), respectively]. Pristine SWCNTs (50 mg) were also immersed without pretreatment and stirred at room temperature in 100 mL of a mixture of HNO_3 (60%) and H_2SO_4 (97%) with a volume ratio of 1:9 for 12 and 48 h [HNO_3/H_2SO_4-12 h (yield 72 wt %) and HNO_3/H_2SO_4-48 h (yield 69 wt %), respectively]. These solutions were filtered through a membrane filter with a pore diameter of 10 μm and then washed with distilled water several times. After the material collected on the filter had been dried in a vacuum for 12 h at 383 K, these samples were further heat-treated in Ar atmosphere for 1 h at 1173 K (heating rate of 90 K min^{-1}).

Characterization. Thermogravimetric analysis (TGA) was conducted in air and was carried out from room temperature to 1273 K with a heating rate of 5 K min^{-1}. Field-emission scanning electron microscopy (FESEM, JEOL JSM6700F) observations were carried out at a 15-kV accelerating voltage. Raman spectroscopy measurements were performed at room temperature under ambient conditions, using a microprobe Raman spectrometer (Renishaw RM1000). The Raman spectra were obtained using excitation lasers with a wavelength of 514 nm (Ar ion laser). X-ray photoelectron spectroscopy (XPS) was carried out using an auger electron X-ray photoelectron spectrometer (VG Microtech, ESCA2000). The measurements were performed with Mg Kα radiation under a vacuum pressure of less than 10^{-6} Pa at room temperature. The pore structures were determined by adsorption of N_2 at 77 K and CO_2 at 273 K using volumetric equipment (Micromeritics ASAP2020), after preevacuation for 12 h at 473 K, while maintaining the base pressure at 10^{-4} Pa. Pore structure parameters were obtained by the subtracting-pore-effect (SPE) and Dubinin−Radushkevich (DR) methods. The SPE method was performed by using high-resolution α_s plots constructed for standard adsorption data on highly crystalline nonporous carbon black.[6,13] We employed the Horvath−Kawazoe (HK) and Barrett−Joyner−Halenda (BJH) methods to determine the micropore and mesopore size distributions, respectively.

Results and Discussion

HNO_3/H_2SO_4 treatments of carbon nanotubes have been frequently used for length-modification and functionalization of nanotubes.[14−17] The volume ratio (1:9) of HNO_3/H_2SO_4 used in the present study provides milder condition because of the lower production rate of nitronium ion (NO_2^+), compared to the typical volume ratio (1:3) used for severe nanotube modification. Moreover, our HNO_3/H_2SO_4 treatment is conducted at lower reaction temperature and without sonication. It is well-known that mixtures of HNO_3 and H_2SO_4, as compared to HNO_3-only solutions, give a higher production rate of NO_2^+, which can easily attack π electrons in aromatic rings.[18]

$$HNO_3 + 2H_2SO_4 \leftrightarrow NO_2^+ + H_3O^+ + 2HSO_4^- \quad (1)$$

The concentration of NO_2^+ produced from a HNO_3/H_2SO_4 solution is strongly dependent on the ratio of HNO_3 and H_2SO_4. Therefore, controlling the volume ratio of the two acids is a key factor in adjusting the mixture's oxidation capability. NO_2^+ (electrophilic group) can attack π electrons on the carbon nanotube surface, which can lead to the strong adsorption of NO_2^+ onto the nanotube surface and subsequent oxidation. Moreover, NO_2^+ adsorption should be promoted by the intercalation of H_2SO_4 into the SWCNT bundles. In this way, defects and O-based functional groups such as −COOH and −OH should be introduced on the caps or side walls of SWCNTs. For the H_2O_2/H_2SO_4 solution used in comparison with the HNO_3/H_2SO_4 treatment, oxygen atoms decomposed from H_2O_2 ($H_2O_2 \rightarrow H_2O + O$) induce an oxidative reaction with nanotube surfaces.[19,20]

(12) Kaneko, K.; Murata, K. *Adsorption* **1997**, *3*, 197.
(13) Murata, K.; Kaneko, K.; Kokai, F.; Takahashi, K.; Yudasaka, M.; Iijima, S. *Chem. Phys. Lett.* **2000**, *331*, 14.
(14) Moon, J. M.; Park, Y. S.; An, K. H.; Park, G. S.; Lee, Y. H. *J. Phys. Chem. B* **2001**, *105*, 5677.
(15) Wiltshire, J. G.; Khlobystov, A. N.; Li, L. J.; Lyapin, S. G.; Briggs, G. A. D.; Nicholas, R. J. *Chem. Phys. Lett.* **2004**, *386*, 239.
(16) Liu, J.; Rinzler, A. G.; Dai, H.; Hafner, J. H.; Bradley, R. K.; Boul, P. J.; Lu, A.; Iverson, T.; Shelimov, K.; Huffman, C. B.; Rodriguez-Macias, F.; Shon, Y.-S.; Lee, T. R.; Colbert, D. T.; Smalley, R. E. *Science* **1998**, *280*, 1253.
(17) Yu, R.; Chen, L.; Liu, Q.; Lin, J.; Tan, K.-L.; Ng, S. C.; Chan, H. S. O.; Xu, G.-Q.; Hor, T. S. A. *Chem. Mater.* **1998**, *10*, 718.
(18) Carey, F. A. *Organic Chemistry*; McGraw-Hill: New York, 1996.
(19) Kang, F.; Leng, Y.; Zhang, T.-Y. *J. Phys. Chem. Solids* **1996**, *57*, 889.
(20) Yang, C.-M.; Kasuya, D.; Yudasaka, M.; Iijima, S.; Kaneko, K. *J. Phys. Chem. B* **2004**, *108*, 17775.

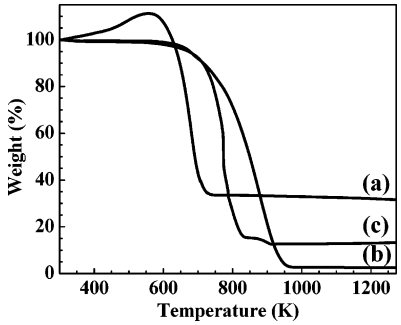

Figure 1. TGA curves of SWCNT samples: (a) pristine SWCNTs, (b) purified SWCNTs, and (c) HNO_3/H_2SO_4-48 h.

TGA was performed to determine the oxidation stability and Fe content of the nanotube samples (Figure 1). The initial weight gain of pristine SWCNTs originates from the oxidation of Fe particles. The residual components after burning at 1273 K are expected to be iron oxides. The Fe content, determined by assuming that the iron oxides are composed of equal amounts of Fe_2O_3 and Fe_3O_4, decreases from 22.2 to 1.7 wt % after purification. The main burning temperature of purified SWCNTs shifts to a higher temperature after purification, which should be associated with Fe content contained in the nanotube sample. It is well-known that many transition metals and their oxides play a catalytic role in the gasification of carbon materials. Consequently, the reduced Fe content after purification results in a weaker catalytic effect on the reactivity of the nanotubes toward oxygen. On the other hand, the Fe content is also reduced after HNO_3/H_2SO_4 treatment for 48 h without purification, but a considerable amount of Fe (9.5 wt %) still remains in the sample. The shift of the burning temperature to higher temperature could also be attributed to the reduced Fe content. Moreover, the enhanced bundle size might partially affect the change of the burning temperature. This effect will also be discussed in relation to the micropore surface area later.

Figure 2 shows FESEM images for SWCNT samples. The pristine and purified SWCNT assemblies are formed by an aggregation of bundles that are about 10 nm in diameter, as shown in Figure 2a,b. The assemblies also show numerous voids because of their large interbundle distance, and as a consequence, they have a low packing density. Such a low packing density should contribute to a high external surface area and larger mesopores of the nanotube assembly, as will be described in the discussion of the gas adsorption results. The H_2O_2/H_2SO_4 treatment of the purified SWCNTs enlarges their bundle size, but the change in interbundle distance is not notable. On the other hand, HNO_3/H_2SO_4-treated SWCNTs before and after purification show a decrease in voids formed between bundles as well as a slight enlargement of the bundle size, and therefore, the packing density is likely to be considerably enhanced.

Figure 3 shows the D-band (1335 cm^{-1}) and G-band (1591 cm^{-1}) regions of the Raman spectra that are attributed to disordered carbon at defects in graphene sheets and the vibration mode of graphite-like carbon, respectively. All samples of Figure 3a were heat-treated in Ar gas ambient at 1173 K after acid treatments. The intensities of the Breit−Wigner−Fano (BWF) shape at the lower-energy side of the

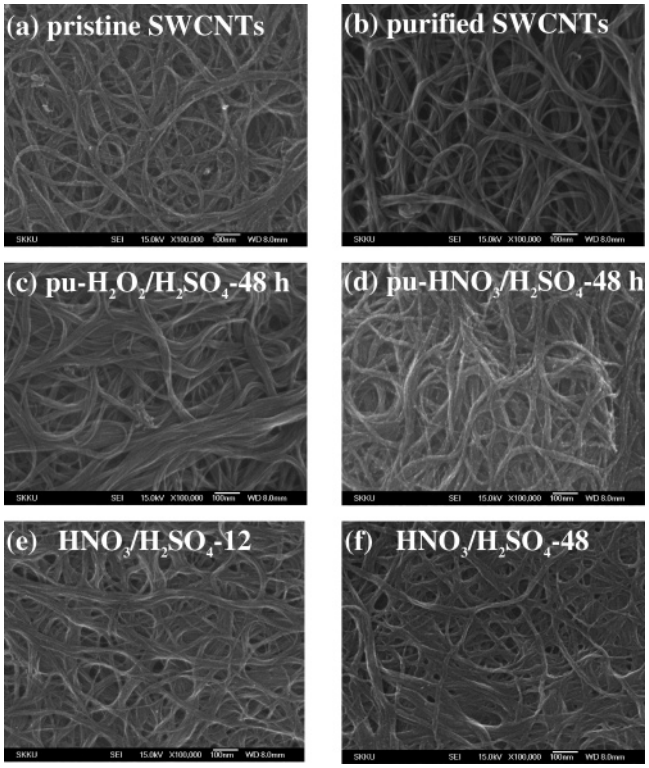

Figure 2. FESEM images of SWCNT samples.

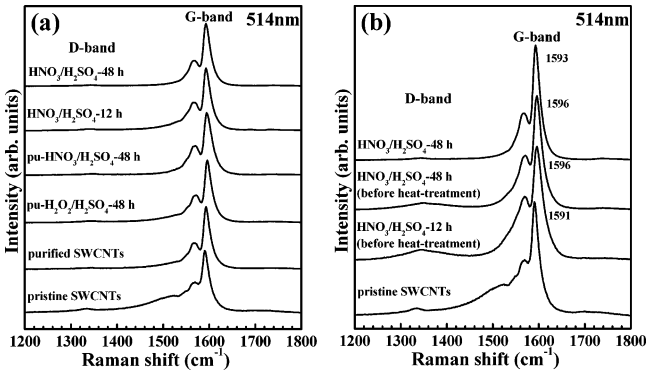

Figure 3. Raman spectra of SWCNT samples: (a) D and G bands of purified and acid-treated samples followed by heat treatment and (b) effect of subsequent heat treatment on D and G bands after HNO_3/H_2SO_4 treatment.

G bands, which originate from metallic SWCNTs, are considerably reduced after purification and acid treatments, indicating the removal of small-diameter metallic SWCNTs.[21] Gas-phase oxidation treatment easily etches and destroys small-diameter SWCNTs because of the higher strain energy caused by their curvature, independent of metallicity,[22,23] whereas HNO_3/H_2SO_4 treatment selectively removes small-diameter metallic SWCNTs (not shown here), as described in detail elsewhere.[24] The intensity ratio of the D band to the G band decreases slightly after purification and acid treatments because of the decreased amount of amorphous

(21) Eklund, P. C.; Subbaswamy, K. R. *Phys. Rew. B* **1979**, *20*, 5157.
(22) Zhou, W.; Ooi, Y. H.; Russo, R.; Papanek, P.; Luzzi, D. E.; Fischer, J. E.; Bronikowski, M. J.; Willis, P. A.; Smalley, R. E. *Chem. Phys. Lett.* **2001**, *350*, 6.
(23) Wiltshire, J. G.; Khlobystov, A. N.; Li, L. J.; Lyapin, S. G.; Briggs, G. A. D.; Nicholas, R. J. *Chem. Phys. Lett.* **2004**, *386*, 239.
(24) Yang, C.-M.; Park, J. S.; An, K. H.; Lim, S. C.; Seo, K.; Kim, B.; Park, K. A.; Han, S.; Park, C. Y.; Lee, Y. H. *J. Phys. Chem. B*, **2005**, *109*, 19242.

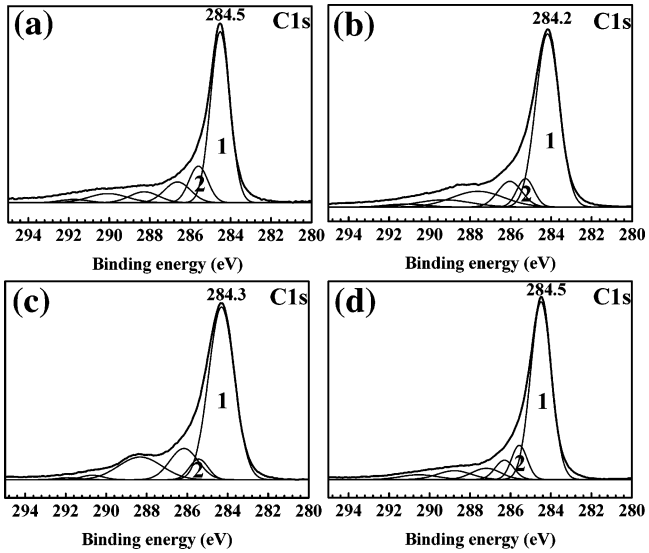

Figure 4. C 1s XPS spectra of SWCNT samples: (a) pristine SWCNTs, (b) HNO_3/H_2SO_4-12 h before annealing at 1173 K, (c) HNO_3/H_2SO_4-48 h before annealing at 1173 K, and (d) HNO_3/H_2SO_4-48 h after annealing at 1173 K.

carbon. Figure 3b shows Raman spectra of HNO_3/H_2SO_4-treated SWCNTs before and after the subsequent heat treatment. The G band of HNO_3/H_2SO_4-treated SWCNTs is upshifted significantly by about 5 cm^{-1} compared to that of pristine SWCNTs, which is attributed to charge transfer between SWCNTs and NO_2^+ (electron acceptor).[25,26] After the subsequent heat treatment, the Raman frequency of the G band is almost recovered. Moreover, the D-band intensities of the SWCNTs increase after HNO_3/H_2SO_4 treatments, indicating intercalation of acid molecules and introduction of functional groups. These intensities are recovered after the subsequent heat treatment because of the elimination of the intercalated molecules and functional groups formed at the defect sites. Therefore, these results suggest that modifications of the SWCNT assemblies by the purification and acid treatments do not cause severe structural destruction in the SWCNT walls.

To confirm the changes in the surface chemistry of the SWCNT samples after HNO_3/H_2SO_4 treatments, we analyzed the XPS spectra. Figure 4 shows the deconvoluted C 1s XPS spectra of the pristine and HNO_3/H_2SO_4-treated SWCNTs. All C 1s XPS spectra consist of six components. Peaks 1 (near 284.5 eV) and 2 (285.6 eV) can be assigned to sp^2-hybridized carbons of nanotube walls and sp^3-hybridized carbons at the defect sites on nanotube walls, respectively. With HNO_3/H_2SO_4 treatments of the pristine SWCNTs, the full width at half-maximum (fwhm) of peak 1 increases considerably with treatment time, accompanied by a slight downward shift in the peak position, as reported in Table 1. This could be attributed to the functionalization and charge transfer induced by an attack of NO_2^+. This broadened peak is almost recovered by the subsequent heat treatment. The integrated area percentage of peak 2 decreases after HNO_3/H_2SO_4 treatments (Table 1), indicating a decrease in the amount of amorphous carbon because of the oxidative etching effect. Peaks near 286−293 eV, which can be assigned to −C−OH, −C═O, −COOH, and −C−N groups,[27] develop as a result of the HNO_3/H_2SO_4 treatments, suggesting the introduction of O- and N-based functional groups. The peaks are reversed after the subsequent heat treatment because of elimination of the introduced functional groups. Figure 5 shows O 1s and N 1s XPS spectra. The O 1s XPS spectra indicate that −C−OH, −C═O, and −C−O−C− groups (near 531−535 eV) develop after HNO_3/H_2SO_4 treatment and are reversed after the subsequent heat treatment. With HNO_3/H_2SO_4 treatment, the N 1s XPS spectra clearly show C−N-related peaks (near 398−403 eV) that could also be removed by the subsequent heat treatment. These results provide evidence that NO_2^+ can attack −C═C− sites of SWCNT walls, thereby introducing C−N- and C−O-related groups on the nanotube surface that are easily eliminated again by the subsequent heat treatment.

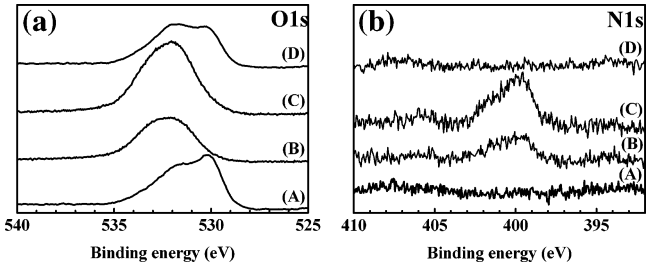

Figure 5. (a) O 1s and (b) N 1s XPS spectra of SWCNT samples: (A) pristine SWCNTs, (B) HNO_3/H_2SO_4-12 h before annealing at 1173 K, (C) HNO_3/H_2SO_4-48 h before annealing at 1173 K, and (D) HNO_3/H_2SO_4-48 h after annealing at 1173 K.

Table 1. C 1s XPS Analysis Results of SWCNT Samples

	peak 1			peak 2	
sample	binding energy (eV)	area (%)	fwhm (eV)	binding energy (eV)	area (%)
pristine SWCNTs	284.5	63	1.13	285.6	13
HNO_3/H_2SO_4-12 h before annealing	284.2	63	1.38	285.3	8
HNO_3/H_2SO_4-48 h before annealing	284.3	65	1.51	285.4	6
HNO_3/H_2SO_4-48 h	284.5	69	1.20	285.6	10

To confirm the packing density of the SWCNT assemblies, we used the gas adsorption technique. Figure 6a shows N_2 adsorption isotherms of the pristine, purified, and H_2O_2/H_2SO_4- and HNO_3/H_2SO_4-treated SWCNTs. The N_2 adsorption isotherm of the pristine SWCNTs is close to type II by the IUPAC classification. The pristine SWCNTs show gradual N_2 uptake at a moderate pressure (P/P_0) and also show a predominant N_2 adsorption at high P/P_0, which is associated with multilayer adsorption on the external surface and macropores. The N_2 adsorption isotherm of purified SWCNTs is also type II. However, it exhibits an enhanced adsorption uptake of N_2 below $P/P_0 = 0.1$, indicating further development of micropores. H_2O_2/H_2SO_4 treatment after purification dramatically increases the N_2 adsorption amount at low P/P_0 without changing the isotherm type. On the other hand, the

(25) Rao, A. M.; Eklund, P. C.; Bandow, S.; Thess, A.; Smalley, R. E. *Nature* **1997**, *388*, 257.

(26) Bandow, S.; Rao. A. M.; Sumanasekera, G. U.; Eklund, P. C.; Kokai, F.; Takahashi, K.; Yudasaka, M.; Iijima, S. *Appl. Phys. A* **2000**, *71*, 561.

(27) Biniak, S.; Szymanski, G.; Siedlewski, J.; Swiatkowski, A. *Carbon* **1997**, *35*, 1799.

Table 2. Pore Structure Parameters of SWCNT Samples Determined by SPE Methods

			microporosity		mesoporosity		
sample	total surface area ($m^2\ g^{-1}$)	total pore volume (mL g^{-1})	micropore surface area ($m^2\ g^{-1}$)	micropore volume (mL g^{-1})	external surface area ($m^2\ g^{-1}$)	mesopore volume (mL g^{-1})	micropore volume percent (%)
pristine SWCNTs	287	0.96	100	0.10	187	0.86	10
purified SWCNTs	524	1.16	336	0.18	188	0.98	11
pu-H_2O_2/H_2SO_4-48 h	932	1.01	734	0.32	198	0.69	32
pu-HNO_3/H_2SO_4-48 h	865	0.35	858	0.32	7	0.03	91
HNO_3/H_2SO_4-12 h	815	0.62	679	0.30	136	0.32	48
HNO_3/H_2SO_4-48 h	890	0.47	857	0.33	33	0.14	70

N_2 adsorption isotherm of SWCNTs treated with HNO_3/H_2SO_4 after purification changes to typical type I with a steep uptake at low P/P_0 and a long plateau at high P/P_0, which are associated with the presence of uniform microporosity and a small amount of external surface, respectively. This result strongly demonstrates that the packing density of the SWCNT assemblies is enhanced by HNO_3/H_2SO_4 treatment. Figure 6b shows N_2 adsorption isotherms of HNO_3/H_2SO_4-treated SWCNTs without purification. After HNO_3/H_2SO_4 treatments, the N_2 adsorption isotherms are intermediate in shape between types I and II, although they exhibit hysteresis loops that can be assigned to types H3 and H4. It is well-known that types H3 and H4 have been generally obtained with platelike particles or slit-shaped pores.[28] In general, platelike particles provide both wedge- and slit-shaped pores. Here, we can consider the SWCNT bundle as a platelike particle. Therefore, the wedge- and slit-shaped pores should be formed in spaces between SWCNT bundles. The N_2 adsorption amount at high P/P_0, which is related to the meso- and macroporosities of SWCNTs, decreases with HNO_3/H_2SO_4 treatment time. Therefore, HNO_3/H_2SO_4 treatment should promote the formation of a densely packed assembly structure by shrinking the wedge- and slit-shaped pores formed between SWCNT bundles. The amounts of larger pores such as mesopores and macropores are directly dependent on HNO_3/H_2SO_4 treatment time. Moreover, the HNO_3/H_2SO_4 treatments dramatically increase the N_2 adsorption amount at low P/P_0, indicating the development of micropores.

To determine the exact porosity, we employed the SPE method using high-resolution α_s plots for the N_2 adsorption isotherms (77 K) of SWCNT samples. The pore-structure parameters of the samples are summarized in Table 2. α_s plots provide information about the total surface area, micropore volume, and external surface area.[6] The mesopore volume was calculated by subtracting the micropore volume from the total pore volume, which was determined from the amount of N_2 adsorbed at $P/P_0 = 0.98$. The purification enhances the microporosity such as micropore surface area and micropore volume without a pronounced change in the external surface area and a significant change in the micropore volume percent. Such a microporosity enhancement by purification is in good agreement with the previous result.[6] After H_2O_2/H_2SO_4 treatment of the purified SWCNTs, the micropore surface area and micropore volume are markedly increased, which is attributed to the partial opening of the SWCNTs and the increase in interstitial space through the formation of the larger bundle structure, whereas the change in external surface area is not notable. On the other hand, the HNO_3/H_2SO_4 treatment of purified SWCNTs markedly increases the total surface area, micropore surface area, and micropore volume, whereas it decreases the external surface area and mesopore volume (to 7 $m^2\ g^{-1}$ and 0.03 mL g^{-1}, respectively). It is important to note that the micropore volume percent dramatically increases from 10% to 91% as a result of the HNO_3/H_2SO_4 treatment for 48 h, indicating a higher packing density. This should be related to a narrow space between bundles as well as a large bundle size of SWCNTs. For the HNO_3/H_2SO_4 treatment of the pristine SWCNTs, the microporosity increases with treatment time, whereas the mesoporosity decreases. Thus, the micropore volume percent progressively increases with increasing treatment time. In particular, the high micropore surface area of 857 $m^2\ g^{-1}$ is obtained after HNO_3/H_2SO_4 treatment for 48 h. It is of note that the micropore surface area and micropore volume increase by about 8.6 and 3.3 times, respectively, after HNO_3/H_2SO_4 treatment for 48 h. Such a considerable difference in the increments of the micropore surface area and micropore volume should stem from the narrowed pore sizes. The purification, H_2O_2/H_2SO_4, and HNO_3/H_2SO_4 treatments are efficient in developing the microporosity of SWCNT assemblies and this developed microporosity provides quantitative information on the bundling and defect formation of SWCNTs. On the other hand, the purification and H_2O_2/H_2SO_4 treatment do not give a pronounced change in mesoporosity, whereas the HNO_3/H_2SO_4 treatment dramatically decreases the mesoporosity. Therefore, HNO_3/H_2SO_4 treatments before and after purification can control the packing density of SWCNT assemblies.

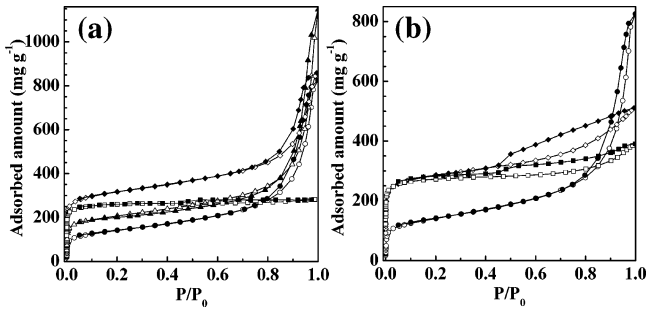

Figure 6. N_2 adsorption isotherms (77 K) of SWCNT samples. The open and solid symbols indicate adsorption and desorption branches, respectively: (a) pristine SWCNTs (○), purified SWCNTs (△), pu-H_2O_2/H_2SO_4-48 h (◇), pu-HNO_3/H_2SO_4-48 h (□); (b) pristine SWCNTs (○), HNO_3/H_2SO_4-12 h (◇), HNO_3/H_2SO_4-48 h (□). All samples were annealed in Ar gas ambient at 1173 K.

(28) Gregg, S. J.; Sing, K. S. W. *Adsorption, Surface Area and Porosity*; Academic Press: London, 1982.

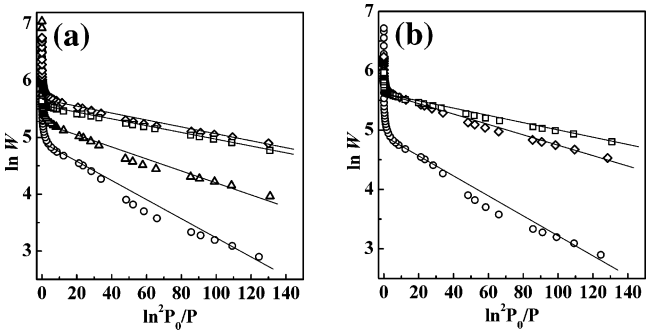

Figure 7. DR plots of N_2 adsorption isotherms (77 K) on SWCNT samples: (a) pristine SWCNTs (○), purified SWCNTs (△), pu-H_2O_2/H_2SO_4-48 h (◊), pu-HNO_3/H_2SO_4-48 h (□); (b) pristine SWCNTs (○), HNO_3/H_2SO_4-12 h (◊), HNO_3/H_2SO_4-48 h (□).

Table 3. Isosteric Heat of Adsorption ($q_{st,\phi=1/e}$), Average Micropore Width (w), and Micropore Volumes (W_0^{N2} and W_0^{CO2}) Determined from DR Plots of N_2 (77 K) and CO_2 (273 K) Adsorption Isotherms

	N_2 at 77 K			CO_2 at 273 K
sample	$q_{st,\phi=1/e}$ (kJ mol^{-1})	w (nm)	W_0^{N2} (mL g^{-1})	W_0^{CO2} (mL g^{-1})
pristine SWCNTs	10.3	1.4	0.13	0.09
purified SWCNTs	11.8	1.1	0.23	–
pu-H_2O_2/H_2SO_4-48 h	13.9	0.8	0.33	0.45
pu-HNO_3/H_2SO_4-48 h	14.0	0.8	0.31	0.39
HNO_3/H_2SO_4-12 h	12.4	1.0	0.33	0.34
HNO_3/H_2SO_4-48 h	13.9	0.8	0.32	0.39

The enhanced bundle diameters might also increase the burning temperature, in accordance with TGA results. The purification dependence of the packing density of HNO_3/H_2SO_4-treated SWCNTs should be related to the presence of Fe that is coated with graphene layers with a diameter of several nanometers, as shown in the TGA results. That is, in the unpurified sample, such particles that are sandwiched between SWCNT bundles might hinder SWCNTs from forming more closely packed assemblies.

Figure 7 shows DR plots for the N_2 adsorption isotherms of the SWCNT samples. All of the DR plots are linear in the low-pressure range. The micropore volumes from the DR equation are given by

$$\ln W = \ln W_0 - (A/\beta E_0)^2, \quad A = RT \ln(P_0/P) \qquad (2)$$

where W is the adsorbed amount at P/P_0, W_0 is the micropore volume, A is the adsorption potential, β is the affinity coefficient, and E_0 is the characteristic adsorption energy. Furthermore, βE_0 gives the isosteric heat of adsorption at a fractional filling ϕ of e^{-1}

$$\beta E_0 + \Delta H_v = q_{st,\phi=1e} \qquad (3)$$

where ΔH_v is the enthalpy of vaporization. We used a liquid density of 0.808 g mL^{-1}, a β value of 0.33, and a ΔH_v value of 5.58 kJ mol^{-1} for N_2 in this analysis. The average micropore width can be calculated from the characteristic adsorption energy

$$(w/2)E_0 = K \qquad (4)$$

where w and K are the average micropore width and a constant, respectively. Values of w and $q_{st,\phi=1/e}$ determined from these DR plots are summarized in Table 3. Purification decreases the w value from 1.4 to 1.1 nm. Subsequent acid

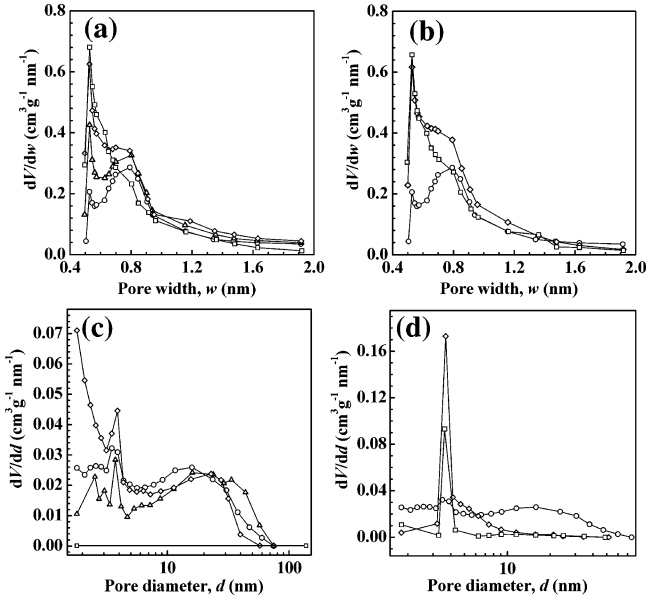

Figure 8. Micropore and mesopore size distributions obtained from N_2 adsorption isotherms (77 K) of SWCNT samples by the HK and BJH methods: (a,c) pristine SWCNTs (○), purified SWCNTs (△), pu-H_2O_2/H_2SO_4-48 h (◊), pu-HNO_3/H_2SO_4-48 h (□); (b,d) pristine SWCNTs (○), HNO_3/H_2SO_4-12 h (◊), HNO_3/H_2SO_4-48 h (□).

treatments of the purified SWCNTs promote the reduction of the w value. For the HNO_3/H_2SO_4 treatment of the pristine SWCNTs, the w values become smaller with increasing treatment time. In general, the $q_{st,\phi=1/e}$ value depends on the pore size and chemical state of the pore wall. That is, a greater $q_{st,\phi=1/e}$ value indicates a stronger adsorbate−pore interaction. The purified SWCNTs show a slightly enhanced $q_{st,\phi=1/e}$ value. On the other hand, the $q_{st,\phi=1/e}$ values for the H_2O_2/H_2SO_4- and HNO_3/H_2SO_4-treated samples show a meaningful increase of 3.6−3.7 kJ mol^{-1} compared to that for the pristine SWCNTs. We attributed these results to the developed microporosity originating from the opening of closed SWCNTs and the enhanced packing density of the SWCNT assemblies.

We also used the HK method to obtain the micropore size distribution. Figure 8a,b shows the micropore size distributions determined by the HK method. The pore size distribution (PSD) of the pristine SWCNTs is mainly in the range of 0.5−1.0 nm, with a shoulder in the range of 1.0−2.0 nm. After purification, the peak intensity from 0.5−1.0 nm increases slightly. On the other hand, the subsequent acid treatments of the purified SWCNTs increase the PSD in the range of 0.4−0.8 nm, suggesting that such treatments develop the narrow microporosity through an increase of the interstitial spaces by the enlarged bundle size and narrowed interbundle distance, as well as the opening of closed SWCNTs. HNO_3/H_2SO_4 treatment is more effective at narrowing the PSD compared to H_2O_2/H_2SO_4 treatment. HNO_3/H_2SO_4 treatments of the pristine SWCNTs considerably enhance the PSDs near 0.5 nm, as shown in Figure 8b. The intensity of the shoulder progressively decreases with HNO_3/H_2SO_4 treatment time. Therefore, the HNO_3/H_2SO_4 treatment can efficiently provide more uniform microporosity to SWCNT assemblies. The mesopore size distributions were also calculated by the BJH method (Figure 8c,d). The pristine SWCNTs show a broad PSD of up to 100 nm. The purified

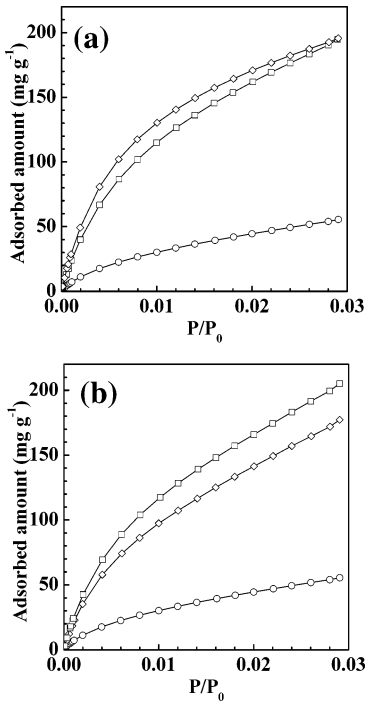

Figure 9. CO_2 adsorption isotherms (273 K) of SWCNT samples: (a) pristine SWCNTs (○), pu-H_2O_2/H_2SO_4-48 h (◇), pu-HNO_3/H_2SO_4-48 h (□); (b) pristine SWCNTs (○), HNO_3/H_2SO_4-12 h (◇), HNO_3/H_2SO_4-48 h (□). All samples were annealed in Ar gas ambient at 1173 K.

and H_2O_2/H_2SO_4-treated SWCNTs do not show a pronounced change in the wide PSDs. On the other hand, HNO_3/H_2SO_4-treated SWCNTs do not give a PSD in the mesopore region, indicating a considerable decrease of the interbundle distance. For HNO_3/H_2SO_4 treatments of the pristine SWCNTs, very uniform mesopore size distributions are obtained at 3.7 nm, and the uniformity enhances with treatment time. Therefore, the PSDs obtained from both the HK and BJH methods clearly demonstrate that the PSDs of SWCNTs are shifted to smaller pore sizes as a result of the HNO_3/H_2SO_4 treatment. The PSDs results are consistent with the pore structure parameters determined by the SPE and DR methods.

We measured CO_2 adsorption (273 K) at subatmospheric pressures up to $P/P_0 = 0.029$, because the saturation pressure of CO_2 at 273 K is extremely high (about 3.5 MPa). CO_2 adsorption at 273 K has been shown to be very effective for the characterization of narrow micropores, because CO_2 at 273 K easily diffuses into very narrow pores because of its larger kinetic energy, whereas N_2 at 77 K shows a restricted diffusion. Therefore, CO_2 adsorption at 273 K has a much greater accuracy than N_2 adsorption at 77 K in microporosity determinations of porous solids. Moreover, according to a previous study, CO_2 adsorption measurements at high pressure revealed that CO_2 adsorption at subatmospheric pressure is a convenient technique for determining narrow micropore volumes.[29] Figure 9 shows CO_2 adsorption isotherms of SWCNT samples. After purification and subsequent acid treatments for SWCNTs, the CO_2 adsorption capacity dramatically increases by about 4 times (Figure 9a). With HNO_3/H_2SO_4 treatments of the pristine SWCNTs, the CO_2 adsorption capacity is considerably enhanced with treatment time (Figure 9b). Therefore, this enhanced CO_2 adsorption capacity should be attributed to the developed ultramicroporosity that can promote the adsorptivity of CO_2. However, we cannot obtain accurate information about the saturated adsorption amounts of CO_2, because CO_2 adsorption measurements were performed in the low-pressure range of $P/P_0 < 0.029$. Consequently, we used the DR analysis for an exact understanding of the pore structure (eq 2; CO_2 density at 273 K of 1.023 g mL^{-1}, β value of 0.35). All DR plots are linear over the entire P/P_0 range (not shown here). The micropore volumes determined from DR plots of the N_2 (W_0^{N2}) and CO_2 (W_0^{CO2}) adsorption results are summarized in Table 3. Garrido et al. classified porous carbons into three groups by comparing W_0^{N2} with W_0^{CO2}: (1) $W_0^{N2} < W_0^{CO2}$, very narrow microporosity; (2) $W_0^{N2} \approx W_0^{CO2}$, relatively narrow and homogeneous microporosity; and (3) $W_0^{N2} > W_0^{CO2}$, wider and heterogeneous microporosity.[30] This classification originates from the different diffusibilities of the two gases. W_0^{CO2} of the pristine SWCNTs is slightly smaller than W_0^{N2}. On the other hand, after acid treatments of the purified and unpurified SWCNT samples, the W_0^{CO2} values are rather large compared to the W_0^{N2} values. In particular, the W_0^{CO2} value (0.45 mL g^{-1}) of the H_2O_2/H_2SO_4-treated sample after purification is much larger than the W_0^{N2} value (0.32 mL g^{-1}). Therefore, a comparison between W_0^{N2} and W_0^{CO2} suggests that acid treatments of the SWCNT samples led to very narrow microporosity through the formation of densely packed assembly structures and the opening of closed SWCNTs.

Conclusions

We have clearly presented a convenient approach for forming densely packed assembly structures of SWCNTs. Gas adsorption techniques have been mainly used to confirm the packed assembly structure of the SWCNTs after acid treatment. Nanoporous materials for application to supercritical gas storage should meet the requirements of high microporosity and high packing density. These requirements could be achieved with the simple HNO_3/H_2SO_4 treatments used in this work. After HNO_3/H_2SO_4 treatment of the purified SWCNTs, the micropore surface area dramatically increased by about 8.6 times, and the micropore volume percent increased from 10% to 91%, indicating formation of a densely packed assembly of SWCNTs. HNO_3/H_2SO_4 treatment could control not only the SWCNT bundle size but also the interbundle distance of the SWCNTs. Control of the interbundle distance was evidenced by hysteresis loops in the N_2 adsorption−desorption isotherms originating from the platelike particles. Moreover, purification of the SWCNTs promoted the formation of a densely packed structure. The enhancement in microporosity and reduction in meso- and macroporosities of the SWCNTs were much more effective compared with those of SWCNHs by the compression method reported previously, as a considerable amount of mesopores was still retained even after the compression of the SWCNHs.[11] The H_2O_2/H_2SO_4 treatment dramatically

(29) Cazorla-Amoros, D.; Alcaniz-Monge, J.; Linares-Solano, A. *Langmuir* **1996**, *12*, 2820.

(30) Garrido, J.; Linares-Solano, A.; Martin-Martinez, J. M.; Molina-Sabio, M.; Rodriguez-Reinoso, F.; Torregrosa, R. *Langmuir* **1987**, *3*, 76.

increased microporosity without a pronounced change of the mesoporosity. On the other hand, the HNO_3/H_2SO_4 treatment dramatically decreased the mesoporosity and increased the microporosity. After the HNO_3/H_2SO_4 treatment, this decrease in the interbundle distance of the SWCNTs should be related to enhanced interbundle interactions due to the charged surface of the SWCNT bundles. Therefore, the difference in mesoporosity change between H_2O_2/H_2SO_4 and HNO_3/H_2SO_4 treatment should be attributed to the stronger oxidation capability of HNO_3/H_2SO_4 solution compared to H_2O_2/H_2SO_4 solution. CO_2 adsorption also indicated that the acid-treated SWCNTs contain very narrow micropores. We expect that these approaches can simply control the packing density as well as the porosity of SWCNT assemblies.

Acknowledgment. This work was supported by the MOST through the New Frontier (TND) project and CNNC at SKKU.

CM0507157